On First Wall and Dust Issues in Fusion Devices

S. I. Krasheninnikov, R. D. Smirnov, D. A. Mendis, and A. Yu. Pigarov

University of California at San Diego, La Jolla, CA 92093, USA

e-mail contact of main author: skrash@mae.ucsd.edu

Abstract. Some critical issues of edge plasma related to the physics of the first wall and dust are discussed. A new model of the formation of "hot spots", often seen in experiments and leading to large impurity influx is considered. A model explaining "fuzz" growth on the Tungsten surface under irradiation of helium containing plasma is proposed. A model allowing simulation of edge plasma transport phenomena with 2D transport codes keeping the most essential features of 3D intermittent edge plasma is described. The limitations for the standard models describing dust grain interactions with plasma are obtained. An impact of non-spherical shape of the grain on dust dynamics is analyzed. The results of first self-consistent simulations of Li dust injection into NSTX performed with coupled DUSTT/UEDGE package are presented.

1. Introduction

The first wall plays crucial role in the design of any fusion reactor. However, the physics of plasma-wall interactions in fusion devices including intermittent edge plasma transport, erosion and modification of wall surface, formation of co-deposited layers, bubbles, "fuzz", dust, etc. (e.g. see Ref. 1-4) is still poorly understood and in many cases there are no even rudimentary models explaining already observed phenomena. Here we address some issues related to the physics of the scrape-off layer transport, first wall, and dust in fusion devices.

2. Wall related physics issues

2.1. On the physics of the "hot spots"

It is known from experiments (e.g. see Ref. 4) that the formation of "hot spots" on the surface of first wall results in significant degradation of plasma performance and, even, termination of the discharge due to large influx of impurity. Most often, "hot spot" observed in long pulse high power shots. Few possible mechanisms of "hot spot" formation are discussed in the literature (e.g. due to thermionic emission), but they are either irrelevant for the conditions available in fusion devices or not directly related to the impurity production seen in experiments. However, there are other overheating mechanism is associated with the temperature dependent desorption of retained in the plasma-facing components (PFC) gas [5]. The desorbed gas is ionized in the vicinity of the PFC increasing the plasma particle and heat fluxes to the surface [6]. In the case of rather high surface temperature the vaporization and ionization of the surface material result in a subsequent return of a part of the vapor to the surface. The incoming vapor particles release at the surface their kinetic and ionization potential energy that leads to

further increase of the surface vaporization. Such mechanism was considered in [7] mainly in application to laser heated materials with Saha type ionization equilibrium assumed in the vapor. The authors, however, did not consider ionization of the vapor by hot background plasma electrons and acceleration of the vapor ions toward the surface by ambipolar electric field formed in the ionization source [6]. These processes are important for PFC heating in fusion grade plasmas and are taken into account in this work.

Because thermionic emission and evaporation are competing mechanisms we need to choose the strongest one. The figure of merit is the ratio of the work function to the evaporation energy of the PFC material. Form the list of fusion relevant material we find that for the case of Be and Li the evaporation mechanism dominates. Then from the PFC heat balance equation we find plasma parameters where thermal bifurcation occurs, which triggers the "hot spot" formation. The results are shown in Fig. 1 [8].
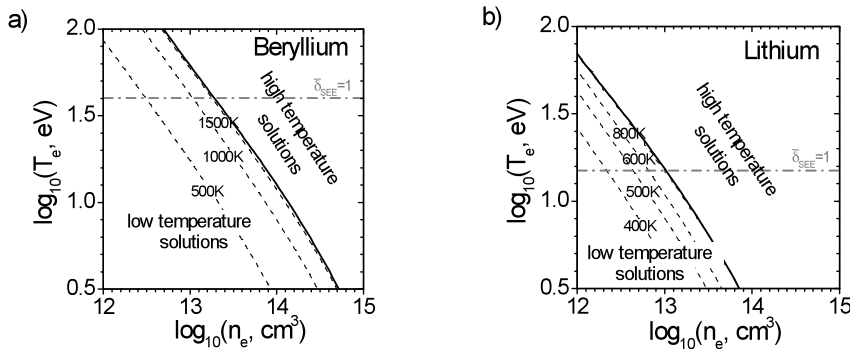

Fig. 1. The calculated low equilibrium temperatures (dashed curves) of the beryllium (a) and lithium (b) PFCs in deuterium plasmas as functions of the plasma parameters. The solid curves indicate the plasma parameters, at which the temperature bifurcation occurs due to the vapor recycling for the surfaces heated up by the plasma.

As we see from Fig. 1, the surface temperature triggering the bifurcation was evaluated as ~800K for Li and as close to melting point ~1560K for Be PFCs. The plasma temperatures and densities, at which the vapor induced thermal bifurcation occurs for these materials, were calculated. The calculated plasma parameters, however, can depend on assumed heat conduction into the material bulk, as well as on inclination of the magnetic field to the surface. The developed model of the surface temperature bifurcation also required that the ionization mean free path of the vapor atoms was smaller than the size of the overheated surface region. This requirement imposed the low limit $\sim 1cm$ on the considered overheated region size for the plasma parameters of interest.

2.2. Visco-elastic model of the "fuzz" growth

Recent experiments on the irradiation of Tungsten with helium-hydrogen plasma [3] have shown the formation of "fuzz", filled with nano-bubbles, on the front surface of the sample. The "fuzz" growth was observed, within some temperature range of the sample, where the thickness of the "fuzz" was increasing as a square root of the time of the irradiation. The rate of "fuzz" growth depends on the temperature of the sample as well as on the rate of helium ion flux. However, at relatively large helium fluxes the rate of "fuzz"

growth saturates. We developed theoretical model describing all main features observed in experiments. This model is based on plastic deformation of the "skin" of the "fuzz" fibers caused by newly growing nano-bubble on the tip of the fiber (see Fig. 2).
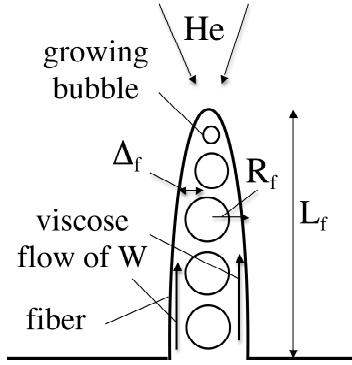

Fig. 2. Schematic view of the fiber.

This model can be described as follows. Newly glowing bubble having high helium pressure inside creates an excessive force on surrounding tungsten "skin" of the fiber and forming pressure difference ΔP between base and nose of the fiber. As a result, tungsten will "flow" through the "skin" from the base to the nose with the speed

$$V_W \sim dL_f/dt \sim \Delta P \Delta_f^2 / L_f \mu_W, \qquad (1)$$

where μ_W is the effective viscosity/plasticity coefficient of tungsten. From Eq. (1) we find the following time dependence of the fiber length

$$L_f(t) \sim \sqrt{2t\Delta P \Delta_f^2 / \mu_W}. \qquad (2)$$

We notice that the thickness of the skin, Δ_f, is fixed by the requirement of no-leakage of helium from other bubbles and, therefore, was assumed to be constant in Eq. (1). We notice that this requirement sets the cap on possible rate of fiber growth and explains saturation of "fuzz" growth with the increase of helium flux to the substrate. Since μ_W has strong temperature dependence, $\mu_W \propto \exp(\Delta E_W / T_W)$, where T_W and the tungsten temperature and ΔE_W is the effective activation energy, from Eq. (2) we find $L_f(t) \sim \sqrt{t}\exp(-\Delta E_W / 2T_W)$. This expression describes both a square root time dependence of "fuzz" growth and strong temperature dependence. From experimental results [3] we deduce $\Delta E_W \sim 1.4\,eV$. Estimate of "fuzz" growth, based on expression (2), gives reasonable agreement with experimental data.

3. Modeling of intermittent SOL transport with 2D edge plasma transport codes

The implementation of diffusion-convection model into UEDGE [9] has allowed significant improvement of 2-D modeling of edge plasma transport accounting for ballisticaly moving blobs. However, still this model is based on the usage of averaged plasma parameters, $\langle p \rangle$, and the functions $F(\langle p \rangle)$ and does not allows to have a strong "bumps" on plasma parameters profiles caused by blobs/ELMs and seen in experiment. Meanwhile, strong fluctuations of plasma parameters, typical for the edge, result in a large departure of $\langle F(p) \rangle$ from $F(\langle p \rangle)$ causing inconsistencies between simulation results and experimental observations and theoretical analysis [10]. In order to overcome this difficulty within the framework of 2D edge plasma transport code (e.g. UEDGE), we are currently implementing into UEDGE a new model allowing strong fluctuations of edge plasma parameters and free from the shortcomings of conventional diffusion-convection approach.

In reality a swarm of blobs, aligned along the magnetic field line, is advected in 3D in radial direction while background plasma moves around the blob in opposite direction. We mimic the 3-D blob motion on the 2-D poloidal cross-section by randomly designating

"patches" (with prescribed statistical properties, which follow from experiment) on poloidal plane, and advecting them with high speed, relevant to blobs, all the way to the wall. This approach better fits experimental observation and allows to describe moving "bumps" on plasma parameter profile.
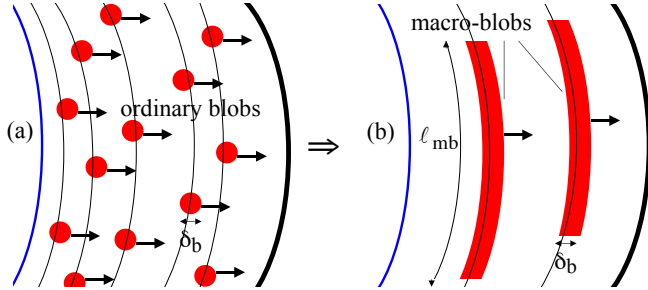

Fig. 3. The poloidal projection of a swarm of ordinary blobs (a) and macro-blobs (b) in the SOL.

However, the calculation of parallel derivatives in 2D transport codes, which assumes toroidal symmetry, is based on poloidal derivatives, which would quickly wash away blob-scale poloidal perturbations. To avoid an unphysical impact of 2D geometry build into the code, we combine the swarms of blobs into "macro-blobs" extended along poloidal directions, Fig. 3. This suppresses erroneous effects of parallel transport and yet preserves all key features of blob dynamics and impact on edge plasma phenomena. We study blob propagation with UEDGE from the core to the chamber for the low-density L-Mode SN shot 105500 on DIII-D. We first obtained stationary plasma profiles assuming only diffusive cross-field transport (D=0.2, χ_e=1.5, χ_i=2 m^2/s). Then, a test blob was initiated as the plasma region (radial size 1.4cm, size along magnetic field line 1.4m for both sides off outer midplane, and at 3cm radially inside separatrix) with uniform cross-field propagation velocity 500m/s. The profiles of plasma density at three different time slices are shown in red on Fig. 4 compared to initial plasma profile. As seen, blob can be clearly indentified as a density spike moving with prescribed velocity. In SOL, blob has a very steep front and a tail. The background plasma density is largely depleted by blob ejection. The ion flux carried by the blob at 4cm in SOL is ~3 kAmp that is large compared to the flux 65Amp in the initial diffusive plasma case. This work is in progress.
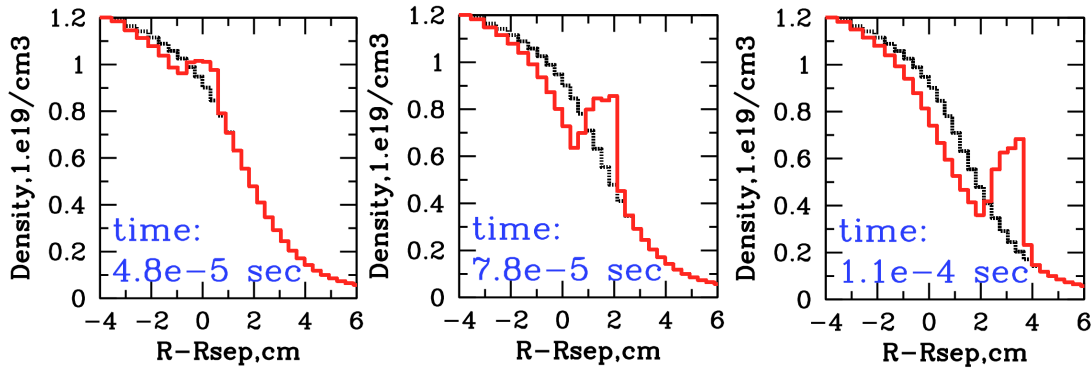

Fig. 4. The results of numerical simulation of plasma density evolution at the outer mid-plane of the DIII-D during the "macro-blob" propagation.

4. Dust related physics issues

In this section we consider the physics of dust-grain interactions for both non-spherical and relatively large grains and discuss the synergetic effects of dust impact on edge plasma parameters and dust dynamics found with self-consistent dust and edge plasma

modeling performed with coupled dust (DUSTT) and edge plasma (UEDGE) transport codes.

4.1. Limitations of available models of dust grain interactions with fusion plasma.

The models used, so far, in the studies of dust-plasma interactions in fusion devices were actually developed for plasma conditions relevant to so-called dusty plasma experiments where both plasma density, n, and temperature, T, are rather low so that the effects associated with the evaporation of the grains can be ignored.

However, in rather dense and hot fusion plasmas this is not always the case. We analyze the effects of the vapor on both the modification of plasma parameters in the vicinity of the grain and plasma-grain interactions. We take into account both vapor-ion collisions and vapor ionization, which produces secondary plasma. Both these effects can alter plasma-grain interactions and can cause the departure electron and ion fluxes on the grain (determining heat fluxes and forces). We find that the effects of grain evaporation can only be ignored for relatively small grain with effective radius $R_d < R_d^{max}(n,T)$. For typical edge plasma parameters and Lithium, Beryllium, and Carbon the functions $R_d^{max}(n,T)$ found from our analysis are shown in Fig. 5 [11]. As we see from Fig. 4, for typical edge plasma parameters $R_d^{max}(n,T)$ appears to be ~10 μm. These results significantly constrain the application of currently used models. For larger grains the effects of vapor can cause both reduction and enhancement of grain-plasma interaction intensity. However, at this time there are no credible theoretical models capable to describe vapor effects for large grains.
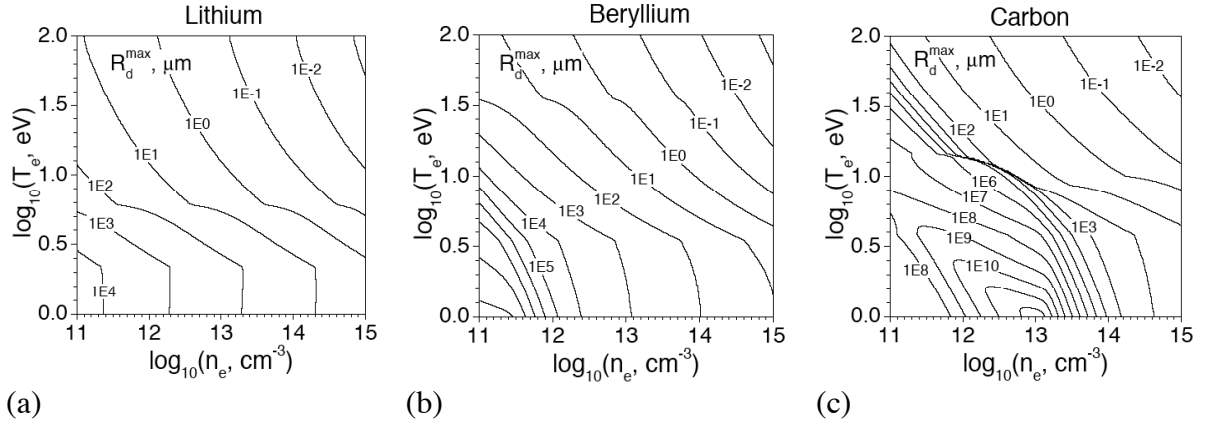

Fig. 5. The contour-plots of $R_d^{max}(n,T)$ for dust material Li (a), Be (b), and C (c).

4.2. Dynamics of non-spherical dust grains in fusion plasma

Another issue with theoretical description of dust-plasma interactions is related to the irregular shape of the grains. So far practically all theoretical studies considered spherically symmetric grains. To address the issues of the impact of grain shape on dust dynamics we review the case where the grain material is solid. Then the grain dynamics is described by 6D equations of motion of a rigid body (e.g. see Ref. 12):

$$M_d d_t \vec{V}_d = \vec{F}_d, \qquad d_t \vec{L}_d = \vec{K}_d \qquad\qquad (3)$$

where M_d is the mass of the grain, $\vec{V}_d$ is the velocity of the grain centre of mass, $\vec{L}_d$ is the grain angular momentum calculated in the frame of the grain centre of mass, $(L_d)_\alpha = I_{\alpha\beta}(\Omega_d)_\beta$, $I_{\alpha\beta}$ is the inertia tensor and $\vec{\Omega}_d$ is the angular velocity of the grain, $\vec{F}_d$ and $\vec{K}_d$ are, respectively, the total force and torque, calculated in the frame of the grain centre of mass, which are imposed on the grain by plasma. In Ref. 13 it was shown that in the absence of electric and magnetic fields, and the effects associated with asymmetric properties of grain material, which can lead to forces and torques (e.g. caused by the "rocket" force), the direction of vectors $\vec{F}_d$ and $\vec{K}_d$ can only depend on the spatial orientation of the grain with respect to the vectors $\vec{W} = \vec{U} - \vec{V}_d$ and $\vec{\Omega}_d$, and both $\vec{F}_d$ and $\vec{K}_d$ vanish for $\vec{W} = \vec{\Omega} = 0$. Since in fusion plasmas grain charging is very fast $\tau_{ch} \sim 10^{-9}$s [14] the inequality $|\vec{\Omega}_d| \tau_{ch} << 1$ holds in a large range of the magnitude of grain angular velocity. For this case, charging processes and the forces imposed on the grain by plasma can be considered in a quasi-stationary approximation. Then for subsonic relative speed W one can keep only linear dependence of both $\vec{F}_d$ and $\vec{K}_d$ on $\vec{W}$ and $\vec{\Omega}_d$. Moreover, if the grain shape does not have intrinsic propeller-like properties, the directions of both $\vec{F}_d$ and $\vec{K}_d$ reverse with reversing directions of $\vec{W}$ and $\vec{\Omega}_d$. As a result, under these assumptions, the expressions for $\vec{F}_d$ and $\vec{K}_d$ can be written as follows

$$(F_d)_\alpha = \Phi_{\alpha\beta}^{(W)}W_\beta + \Phi_{\alpha\beta}^{(\Omega)}(\Omega_d)_\beta, \qquad (K_d)_\alpha = T_{\alpha\beta}^{(W)}W_\beta + T_{\alpha\beta}^{(\Omega)}(\Omega_d)_\beta, \qquad (4)$$

where the tensors $\Phi_{\alpha\beta}$ and $T_{\alpha\beta}$ are determined only by the shape of the grain and plasma parameters.

In general case the calculation of the tensors $\Phi_{\alpha\beta}$ and $T_{\alpha\beta}$ is only possible numerically. However, for the grains having rotationally symmetrical, around some axis, properties the structure of these tensors can be found just from symmetry arguments [13]. In this case spatial orientation of the grain can be characterized by dimensionless vector $\vec{D}$, which is directed along symmetry axis. Then, taking into account that $\vec{F}_d$, $\vec{W}$, and $\vec{D}$ are the vectors, while $\vec{L}_d$, $\vec{K}_d$ and $\vec{\Omega}_d$ are the pseudo-vectors, it was shown that taking into account that in practice $\Omega_d << W/R_d$ and $|\vec{U}| >> |\vec{V}_d|$, the equations (1) can be written as

$$M_d d_t \vec{V}_d = \Phi_1^{(W)}\vec{U} + \Phi_2^{(W)}\vec{D}(\vec{D}\cdot\vec{U}), \qquad d_t\vec{L}_d = T^{(W)}(\vec{U}\times\vec{D}) \qquad (5)$$

In Eq. (5) the scalars $\Phi_1^{(W)}$, $\Phi_2^{(W)}$, and $T^{(W)}$ are determined by particular properties of the grain and plasma parameters and can be estimated (for the grains not too far from spherical shape) as $\Phi_1^{(W)} \sim \Phi_2^{(W)} \sim \hat{F}$, $T^{(W)} \sim \hat{F}R_d$, where $\hat{F} = \xi_F \pi R_d^2 nT/C_s$, $C_s = \sqrt{T/m_i}$, and $\xi_F \sim 10$ is the form-factor depending on the ratio of the Debye length to the grain size. As one sees from Eq. (5): a) the force balance equation has the component which is not aligned with plasma velocity (see also Ref. 15) and b) the angular momentum balance equation is identical to the equation describing the motion of symmetrical top with fixed lowest point in effective gravity field $\propto \vec{U}$ (e.g. see Ref. 12) and, as it is well known, the orientation of vector $\vec{D}$ will oscillate in time. As a result of these oscillations the force on the grain, and therefore, the grain trajectory will experience

some oscillations caused by the second term in the RHS of the momentum balance equation in Eq. (5), which is due to non-spherical shape of the grain. However, in Ref. 13 it was shown that the magnitude of dust trajectory oscillations, Δ_d, can only be significant if the grain spins around the symmetry axis with appreciable angular velocity, Ω_0. In this case for small α, the dust trajectory oscillations Δ_d can be estimated as

$$\Delta_d \sim \frac{\Phi^{(W)}}{M_d U}\left(\frac{I\Omega_0}{T^{(W)}}\right)^2 \sim \frac{M_d \Omega_0^2}{\pi \xi_F n T}\frac{C_s}{U}. \tag{6}$$

From Eq. (6) for $\sim 10 \ \mu m$ grain, $\Omega_0 \sim 10^6 s^{-1}$ and plasma parameters rather typical for the edge of fusion devices $n \sim 3 \times 10^{13} cm^{-3}$, $T \sim 10$ eV, and $U \sim C_s$ one finds that $\Delta_d \sim 1 \ cm$, which can be visible with fast cameras. This estimate shows that the main features of the dynamics of rapidly spinning non-spherical grain can significantly differ from that of spherical one.

4.3. Coupled DUSTT-UEDGE modeling

Even rather small amount of dust can significantly alter impurity concentration and, therefore, edge plasma parameters. On the other hand dust penetration into plasma and, therefore, impurity pollution depend on plasma parameters. Thus, dust dynamics and plasma transport should be treated self-consistently. Here we report on the first results of dust-edge modeling with coupled DUSTT-UEDGE package.

The DUSTT code simultaneously solves equations of motion, charging, heating and ablation for dust particles that are being accelerated, charged and destroyed in fusion plasmas due to various dust-plasma interaction processes [16]. The plasma parameters and the computational mesh for the DUSTT simulations are provided by the edge plasma transport code UEDGE, which solves toroidaly symmetric 2D multi-fluid transport equations for plasma and impurity ions, together with a set of transport equations for hydrogen and impurity atoms [17]. The coupling of the DUSTT and UEDGE codes was performed using scriptable interactive BASIS framework that allows user control of convergence of the iterations. To assess effects of dust on edge plasma performance, we model injection with various rates of lithium dust in fusion plasmas similar to that produced in NSTX tokamak. The core heating power is set at 3MW. The deuterium gas source equivalent to 1000A of ionized atoms is distributed along the wall in the inner-upper quadrant. The low recycling regime is achieved by setting low plasma recycling coefficient at the divertor plates, $R_{plate} = 0.8$. The dust particles are assumed to have log-normal distribution of their radii with the mean radius $\langle R_d \rangle = 22 \ \mu m$ and the standard deviation equal 11 μm. The dust injection velocities are cosine distributed relative to the vertical, $-Z$, direction and are biased downward with the most probable speed $V_p = 5 m/s$. The dust source is assumed to be toroidaly symmetric and located in the outer-upper poloidal quadrant with the dust hitting the plasma at approximately half the way between the outer midplane and the top poloidal locations. Simulations show that the dust injection with rates ~ 10 mg/s can lead to significant increase of impurity concentration and radiation power losses, reduction of the plasma temperature, and significant reduction of the power load to the outer divertor plate (see Fig. 6a) and complete plasma detachment in the inner divertor. Lithium injection also caused substantial $\sim 40\%$ decrease of the radial

plasma pressure gradients at the edge (see Fig. 6b), which can significantly improve peeling/ballooning stability of the edge plasma suppressing anomalous transport and ELM formation. These results are in accord with the observed disappearance of ELMs during lithium dust injection experiments on NSTX [18]. It has been shown that injection of equivalent amount of atomic impurities have qualitatively similar effects on edge plasmas, which, however, are much smaller in magnitude and affect mostly the far SOL regions as compared to the dust.
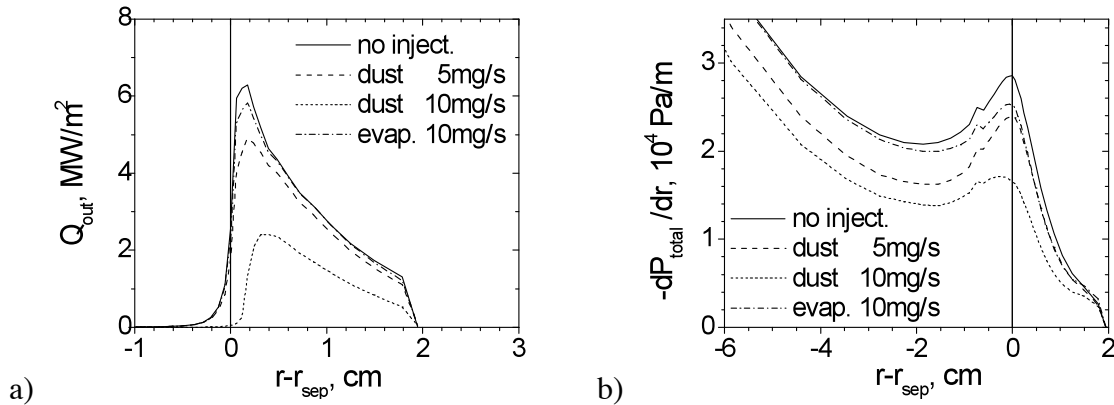

Fig. 6. a) The simulated profile of the plasma heat flux to the outer divertor plate for the different dust/vapor injection rates. Coordinate *r* is mapped to the outer midplane; b) The simulated radial profiles of the radial gradient of the total plasma pressure.

References
1. A. Loarte, et al., Nucl. Fusion **47** (2007) 5203
2. S. I. Krasheninnikov, et al., Plasma Phys. Control. Fusion **50** (2008) 124054
3. M. J. Baldwin, and R. P. Doerner, Nucl. Fusion **48** (2008) 035001 R.S. Kajita et al., Nucl. Fusion **49** (2009) 095005
4. A. Ekedahl, et al., 22nd IAEA FEC, 2008, paper EX/P4-2
5. S. I. Krasheninnikov and T.K. Soboleva, Phys. Plasmas **13** (2006) 094502
6. S. I. Krasheninnikov and R. Chodura, Contrib. Plasma Phys. **34** (1994) 210
7. A. V. Nedospasov and B. P. Shelyukhaev, High Temperatures **28** (1990) 24
8. R. D. Smirnov, et al., Phys. Plasmas **16** (2009) 122501
9. A. Yu. Pigarov, et al., Phys. Plasmas **9** (2002) 1287
10. S. I. Krasheninnikov, et al., Phys. Plasmas **16** (2009) 014501
11. S. I. Krasheninnikov and R. D. Smirnov, Phys. Plasmas **16** (2009) 114501
12. L. D. Landau and E. M. Lifshits, "Course of Theoretical Physics, Vol. 1 Mechanics"
13. S. I. Krasheninnikov, Phys. Plasma **17** (2010) 033703
14. S. I. Krasheninnikov, et al., Phys. Plasmas **11** (2004) 3141
15. S. I. Krasheninnikov and D. A. Mendis, J. Plasma Phys., Pub. online 10 March 2010
16. R. D. Smirnov, et al., Plasma Phys. Control. Fusion **49** (2007) 347
17. T. D. Rognlien, et al., J. Nucl. Mater. **196-198** (1992) 347
18. R. Maingi, et al., Phys. Rev. Lett. **103** (2009) 075001